https://doi.org/10.3311/PPch.44178

Periodica Polytechnica Chemical Engineering

Hydraulic Resistances of Membrane Filters and their Role in Industrial-Scale Make-Up Water Treatment

Qais Tareq Adeeb Al-Madanat[1], Reem Shaheen[1], Edit Cséfalvay[1*]

[1] Department of Energy Engineering, Faculty of Mechanical Engineering, Budapest University of Technology and Economics, Műegyetem rpk. 3. Budapest, H-1111, Hungary
[*] Corresponding author, e-mail: csefalvay.edit@gpk.bme.hu

Received: 31 March 2026, Accepted: 05 June 2026, Published online: 11 September 2026

Abstract

This study presents the design and evaluation of a multistage membrane filtration system to produce ultrapure quality make-up water for thermal power plants using the Danube River as the feedwater source. Laboratory-scale filtration experiments were performed using a flat-sheet test cell to determine the hydraulic resistances of ultrafiltration, nanofiltration, and reverse osmosis membranes under varying transmembrane pressures. The experimental results confirm a linear correlation between the applied pressure and the permeate flow rate for all three membrane types under the tested conditions and establish a resistance-in-series model that provides the basis for upscaling calculations. The flow rate requirement for a single block of Paks power plant is 26.1 m^3/h of ultrapure water, using 90% recovery per membrane stage. Two-stage microfiltration was applied to sufficiently remove the suspended solid content from raw water. The proposed system comprises ultrafiltration, nanofiltration, two-stage reverse osmosis, and electrodeionization, achieving a cumulative recovery of 53.14% and requiring a raw water feed of 49.11 m^3/h. To drive the process, 5 centrifugal pumps were selected across different pressure zones (3, 9, 20, 31, 35 bar), with a total shaft power of 132.6 kW, corresponding to a specific energy consumption of 5.079 kWh/m^3. This research provides a viable framework for scaling laboratory membrane setup to industrial pure water production, underscoring the necessity of an abundant feedwater source to compensate for the tradeoffs in multi-stage recovery.

Keywords

ultrapure water, make-up water, multistage membrane filtration, hydraulic resistance, industrial scale-up

1 Introduction

In spite of having an increased amount of renewable energy, thermal power plants still have a significant role in energy generation, exhibiting the need for ultrapure water using environmentally benign methods [1]. A previous study proposed and evaluated a multistage membrane filtration system designed to produce pure water from the Danube River at laboratory-scale. The proposed technology comprises a pretreatment stage and a desalination stage, which is supplemented by a post-treatment stage to achieve ultrapure water, the working fluid of thermal power plants. The pre-treatment step includes a particle filtration membrane that protects the 0.45 µm pore-size microfilter, followed by an ultrafilter for total organic matter removal, and a nanofilter for partial desalination. The desalination stage consists of two steps of reverse osmosis (RO), which can provide purified water with a conductivity of 2 µS/cm [2]. Further experiments were conducted to observe recovery rates of this sequential configuration. It was proposed to use electrodeionization (EDI) in the post-treatment stage to produce ultrapure water for the power industry as make-up water.

1.1 Driving force of membrane filtration

The driving force of membrane filtration is called transmembrane pressure (TMP), but it is defined differently when using microfiltration (MF), ultrafiltration (UF), nanofiltration (NF), and reverse osmosis [3].

1.1.1 Microfiltration and utrafiltration

In microfiltration and ultrafiltration, TMP equals the applied pressure across the membrane (p):

$$\mathrm{TMP} = \Delta p = \left(p_f - p_p \right), \tag{1}$$

Cite this article as: Al-Madanat, Q. T. A., Shaheen, R., Cséfalvay, E. "Hydraulic Resistances of Membrane Filters and their role in Industrial-Scale Make-Up Water Treatment", Periodica Polytechnica Chemical Engineering, 2026. https://doi.org/10.3311/PPch.44178

where p_f represents the pressure on the feed side, and p_p represents the pressure on the permeate side, given in the same unit [Pa].

In ultrafiltration, the effect of osmotic pressure is usually negligible, even if the concentrations of larger molecules, such as proteins and sugars, are different in the feed and permeate [4, 5].

The influence of osmotic pressure can be significant when the concentration of low-molecular-mass solutes, such as salts, is different on each side of the membrane [4, 6].

1.1.2 Nanofiltration and reverse osmosis

When considering nanofiltration and reverse osmosis, salt solutions are treated, which possess osmotic pressure [7]; therefore, higher pressure is required to overcome it. In this manner, the TMP is the difference between the applied pressure difference (Δp) and the osmotic pressure difference ($\Delta\pi$):

$$\mathrm{TMP} = \Delta p - \Delta\pi = \left(p_f - p_p\right) - \left(\pi_f - \pi_p\right), \tag{2}$$

where π_f is the osmotic pressure on the feed side, and p_p is the osmotic pressure on the permeate side, given in the same measurement unit [Pa] [6].

At a higher TMP, the driving force is increased towards the membrane, leading to a higher permeate flux (J_V, [m^3/(m^2 s)]) [8]. In general, the Darcy equation describes the filtration phenomena [9], and it is valid for the hydrodynamic process of separating solid particles from liquids, as in microfiltration:

$$J_V = \frac{1}{A_m}\frac{dV}{dt} = A \cdot \Delta p, \tag{3}$$

where A is the membrane permeability [m/(s·bar)], V is the volume of the filtrate [m^3], t is the filtration time [s], A_m is the area of the membrane [m^2], and Δp is the pressure difference across the membrane [bar]. When suspended solids are filtered in dead-end mode, an additional layer, the cake, forms, increasing resistance and lowering flux [10].

1.2 Limiting flux

In case of ultrafiltration, Eqs. (1) and (3) are still valid, taking into consideration that when the membrane retains organic materials, they are concentrated on the feed side of the membrane. Fig. 1 shows that at very low pressure, the flux is close to the pure water flux at the same pressure. As the pressure increases, fouling begins to indicate that the critical flux has been exceeded, indicating a critical pressure

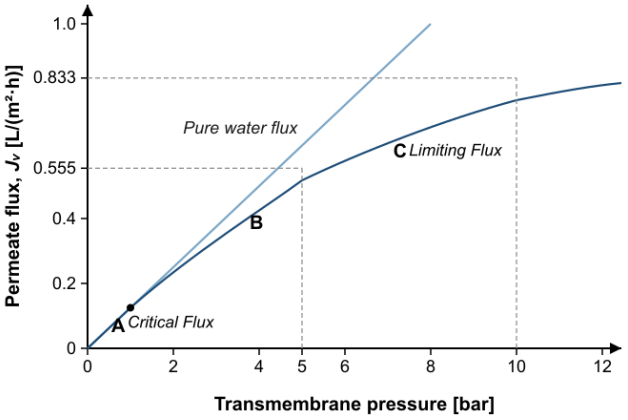

Fig. 1 Permeate flux as a function of transmembrane pressure (TMP) adapted from Aguirre-Montesdeoca et al. [10]

(region A). As the applied pressure increases towards, flux increases; as a consequence of higher flux, concentration polarization takes place, and gel layer formation of the retained material at the membrane surface begins [8]. As the gel layer grows along the membrane, partially covering it, a nonlinear dependence of the flux on pressure occurs (region B – Transition region). Once a gel layer has formed, further increases, so applied pressure does not result in a corresponding increase in permeate flux. Finally, when the gel layer has covered the entire membrane length, the limiting flux is reached, and the flux becomes independent of the pressure (region C) [11]. Considering the work of Aguirre-Montesdeoca et al., the limiting flux was reached in the range of 5-10 bar, which is the maximum steady-state permeate flux (between 0.555–0.833 L/(m^2·h)) is achievable by increasing the TMP in the system [10].

In this manner, the optimal operating parameters, such as pressure, operation time, recovery, *etc*., must be carefully set.

1.3 Role of osmotic pressure

As one proceeds towards suspended solid and organic-content-free solutions, dissolved ions play a role in nanofiltration and reverse osmosis. Due the presence of ions, the transport of water through the membrane is determined, so permeate flux can be observed only when applying a pressure difference higher than the osmotic pressure difference. Increasing the applied pressure influences the permeate flux proportionally, as illustrated in Fig. 2 [12].

1.4 Resistance in membrane filters

The blocked membrane and the foulants can be modeled as resistances in series, (including: all resistances originating from the exposure of the membrane to a solution

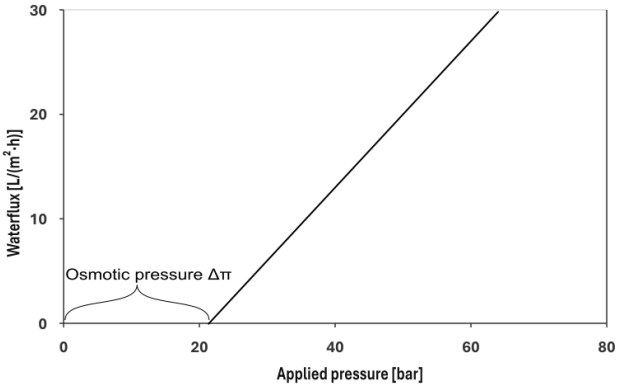

Fig. 2 The relation between permeate flow rate and the pressure drop through the membrane adapted from Wijmans et al. [12]

containing foulants, due to concentration polarization, adsorption, gel layer formation, internal pore fouling, external deposition, or cake formation) derived from Darcy's law. All of the resistances can be summed up as a total resistance.

Within this model, the UF flux rate is related to the total resistance and transmembrane pressure [13–16]:

$$J_v = \frac{\mathrm{TMP}}{\mu \cdot \left(R_m + R_f\right)} \tag{4}$$

where μ is the dynamic viscosity of the filtrate [Pa·s], R_m [1/m] represents the membrane resistance and R_f [1/m] represents the fouling resistance which includes all the kinds of resistances listed above [4]. Membrane fouling leads to a significant increase in total resistance (R_T), which is observed as a gradual decline in permeate flux during constant-pressure operation, or in constant-flux operation, a requirement to increase TMP to maintain constant flux, as seen in Eq (5) [8]:

$$J_v = \frac{\mathrm{TMP}}{\mu \cdot R_T}, \tag{5}$$

where R_T is the total resistance [1/m] to permeation through the membrane. This comprises R_m and R_f.

The rapid initial drop in permeate flux can be attributed to the rapid blocking of membrane pores. The maximum permeate flux occurs at the beginning of filtration because the membrane pores are clean and open. Flux declines as membrane pores are blocked by retained particles. Further flux decline after pore blockage is due to the formation and growth of a cake/gel/foulant layer on the membrane surface. This layer forms on the membrane surface as the amount of retained particles increases, adds additional resistance to permeate flow, and its resistance increases with its thickness. Consequently, the permeate flux continues to decrease over time [8].

The intrinsic membrane resistance R_m is derived from the slope of the flux-pressure curve obtained with pure water as the reference feed and permeate, to establish the absence of particle-induced resistance and the formation of a concentration polarization layer and any kind of fouling [6]. During filtration of real feed water, however, particles interact with the membrane and increase the overall resistance through several fouling mechanisms, including complete blocking, standard blocking, intermediate blocking, and cake formation – as illustrated in Fig. 3.

Membrane resistance can be determined from measurements of pure water volumetric flux. When pure water, with no dissolved content, is fed to all types of membranes, the driving force is exclusively the applied pressure, i.e., the pressure difference between the feed and permeate sides. Moreover, no concentration on the feed side can be observed, so that no concentration polarization could be detected, nor fouling on the membrane surface.

The relation between the volumetric flux and driving force is linear; the proportionality is determined by the multiplication of membrane resistance, and viscosity of the pure water on the permeate side, see Eq. (6).

$$J_v = \frac{\Delta p}{\mu \cdot R_m} \tag{6}$$

Tanninen and coworkers evaluated the flux profile of two RO and one NF membranes for the filtration of deionized water and the bioreactor effluent with high-ionic content [17]. The flux–pressure profiles showed a linear trend with increasing pressure during the filtration of deionized water within the pressure range studied. However, during

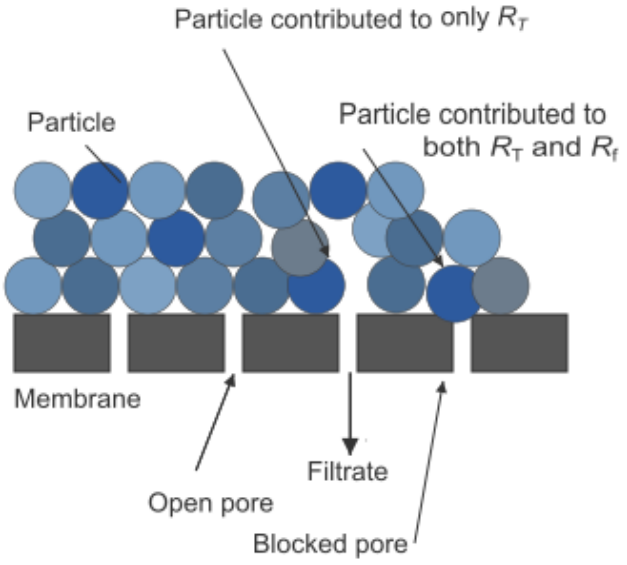

Fig. 3 Mechanism of pore blocking adapted from Iritani [13]

the filtration of bioreactor effluent, after a critical pressure was reached, the rate of increase in flux decreased with increasing pressure for the two RO membranes tested. The flux–pressure profiles observed indicated that the membrane resistance is pressure-dependent and is not linearly correlated with transmembrane pressure for filtration of concentrated solutions and high transmembrane pressures [17].

1.5 Pump flow rate

In an industrial-scale membrane filtration system, feed flow is supplied by pumps whose operating pressures are selected to match the TMP required at each stage. To ensure stable operation, the pump must operate within the linear zone of the pressure drop–flow rate curve related to the membrane. When dealing with laminar flow, the relationship between flow rate and pump pressure drop is linear; in turbulent flow, it is quadratic, meaning the pump has to deliver the fluid according to that relation.

From a hydraulic perspective, two types of equations can be used depending on the flow. In laminar flow, the volumetric flow rate (Q) is low and shows a linear relationship with the pressure drop across the pump. In turbulent flow, the pressure drop shows a quadratic relationship with the volumetric flow rate Q^2 delivered by the pump.

Fig. 4 illustrates the relationship between the pressure drop and the flow rate of the pump, as the flow rate increases, the pressure drop increases linearly in the laminar range. A shift is visible in the case of the transition region between the boundaries of the laminar and turbulent flow [18]. As the flow rate represents a turbulent flow,

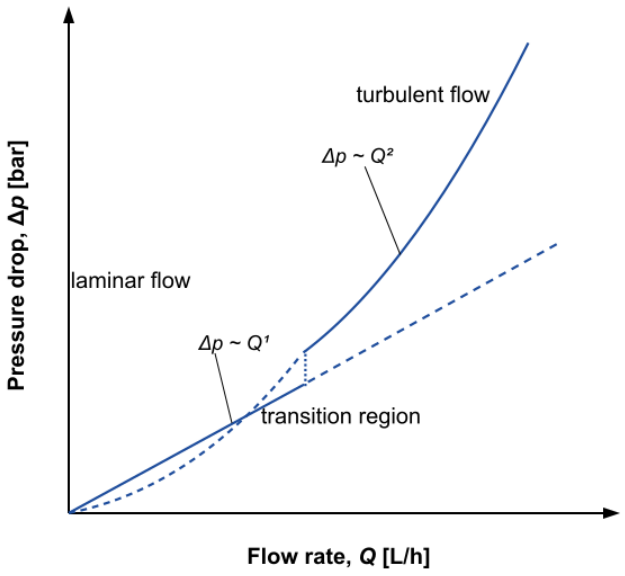

Fig. 4 The relation between the pressure drop of the pump and the flow rate adapted from Maczyszyn [18]

the pressure drop of the pump follows a quadratic relation with the pump flow rate. This study aims to highlight the relationship between flux (i.e. flow rate through 1 m^2 size membrane) and applied pressure across selected ultrafiltration, nanofiltration, and reverse osmosis membranes to verify their linearity. Additionally, it seeks to examine the correlation between applied pressure and the total resistance for these membranes to determine the optimal pressure for higher fluxes. The total resistances derived from experiments are treated as hydraulic resistances which must be come over by the pumps. A linear relationship between hydraulic resistances and applied pressures can lead to design a proper pure-water-producing membrane filtration system at industrial scale for the Danube water. Hydraulic calculations and pump selections are provided.

2 Materials and methods

As a very first step, a qualitative filter paper (Grade No. 413, particle retention of 5-13 μm) was used as the microfiltration membrane to remove the major part of particles [19]. This initial experimental step was conducted in a dead-end configuration with an effective filtration area of 38.5 cm^2. A vacuum was applied to the permeate side of the membrane at 0.59 bar, and the feed side was maintained at atmospheric pressure (≈1.01325 bar). Following this dead-end pretreatment, a sequence of membrane filtration experiments (MF-II, UF, NF, RO-I and RO-II) were carried out on a test membrane unit (CM-CELFA AG P_28, Membrantrenntechnik AG, Switzerland) in crossflow mode, with liquid circulation on the feed side via a circulation pump. According to the manual, the circulation pump delivers 1.81 L/min at 8 bar. The active area of each membrane was 28 cm^2. Membranes were conditioned prior to first use by soaking in distilled water for 1 day. To remove suspended solids from the Danube water, samples were treated with a first Pall Lab SuporTM-450 microfiltration membrane (Pall Corporation, USA, designed for laboratory applications only). Then a series of batch filtrations: ultrafiltration, followed by nanofiltration and reverse osmosis, were tested to determine the hydraulic resistance of the membranes. The series of consecutive steps was repeated three times, and 500 mL of Danube water was used in each experiment series. After pouring the feed into the tank, overpressure was set using a nitrogen gas reducer. During the experiment, permeate continuously left the equipment, and the measuring time was recorded for each 10 mL of permeate to calculate the permeate flux through the membrane. Recovery – defined as the volume of permeate

divided by the initial feed volume – was set at 90%, 90%, and 85% for UF, NF, and RO, respectively. The characteristics of the selected membranes (Sterlitech Company, USA) used in the filtration stages are shown in Table 1 [20].

Water samples were taken on 23rd February 2024 at Műegyetem rakpart, Budapest, and stored at room temperature (~25 °C) before use. The specific electric conductivity (later on conductivity or K) of Danube water 400 µS/cm was measured with a 340I type WTW combined pH/conductivity meter (pH/Cond 340i, WTW GmbH, Germany). The total suspended solid content (TSS) was measured with a Secomam Pastel UV analyser (Secomam SA, France), in the wavelength range of 200–320 nm.

Regarding permeate viscosity, the data were obtained from the international formulation for H_2O viscosity based on permeate temperature and operating pressure [21].

Another series of experiments using Danube water (collected on 6th November 2023) aimed to provide operational parameters for an industrial-scale-designed system, based on lab-scale experiments to produce pure water. Ion concentrations in Danube water and permeate samples after each filtration step carried out at the highest applied pressure (using a conservative approach, that highest ion concentrations could be observed at higher pressures) were measured in mg/L using ion chromatography (Metrohm 861 Advanced Compact IC equipped with Metrohm 837 IC Combi Degasser and Metrohm 838 Advanced Sample Processer provided by Metrohm Company, Switzerland). Based on the measured concentrations, rejection values were calculated to determine efficiency and published in previous work [22].

All experiments in the pretreatment stage (MF-I, MF-II, UF, and NF) and the first desalination stage (RO-I) were carried out and repeated three times. During MF-II, UF, NF and RO experiments, constant temperature of 25 °C was maintained by a SC100 A10 type thermostat (Thermo Fisher Scientific, Hungary).

Our approach is to prove a continuous treatment of surface water, and protect and elongate the lifetime of the reverse osmosis membranes in the desalination stage. As more pretreatment stages are inserted, the fractional removal of original components can be achieved, which reflects a lighter load for each membrane compared to a single stage pretreatment. A typically used single stage UF as pretreatment can lead to fouling of the UF membrane requiring more frequent cleaning, moreover, it would represent a denser feed (i.e. higher ion containing feed) for the reverse osmosis membrane [23], making the desalination stage more complex and longer. Therefore, a relatively high number of steps were used to pretreat the surface water. The scheme of the tested cascade membrane treatment system is shown in Fig. 5.

3 Results and discussion

Table 2 shows a summary of the average values of conductivity and TSS measured after each treatment step. The improvement of ion removal is verified by the continuously decreasing values of the conductivity reaching the detection limit of our equipment after RO-II. TSS was also continuously decreasing along the treatment steps, and the detection limit was reached in the permeate of the nanofiltration step. This verifies the successful removal of the fouling components which protects the membranes from fouling during the next treatment stage. Considering the salt removal from raw Danube water conductivity values were used for the calculation; by the end of the RO-II 99.54% of the ions were removed, which verifies the sufficient operation of the cascade membrane system.

Table 1 Membranes used in hydraulic resistance experiments under different applied pressures

Membrane	Type	Polymer	Applied pressure [bar]	MMCO* [g/mol]	Salt rejection%
UF	GH	EDI	4, 6, 8, 10	2500	-
NF	DL	Polyamide-TFC	14, 16, 18, 20	150-300	96 $MgSO_4$
RO	AG	Polyamide-TFC	25, 28, 31, 35	-	99.5 NaCl

*Molecular mass cut-off.

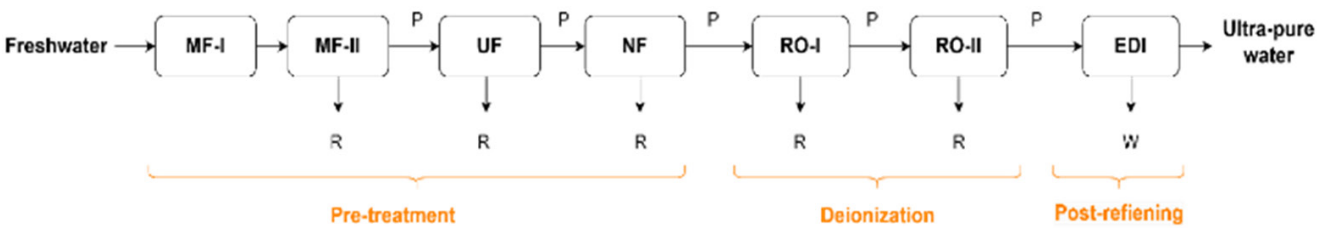

Fig. 5 Lab scale membrane filtration for pure water production followed by an EDI unit to achieve ultrapure water; MF: microfiltration, UF: ultrafiltration, NF: nanofiltration, RO: reverse osmosis, EDI: electrodeionization, P: permeate, R: retentate, and W: waste

Table 2 Stage-by-stage water quality progression

Stage	Conductivity (μS/cm)	TSS (mg/L)	Cumulative *K* removal (%)
Raw Danube	438	53.60 ± 2.51	—
After MF-I	436	32.40 ± 3.78	0.46
After MF-II	392	13.40 ± 1.82	10.50
After UF	383.5 ± 3.7	11.45 ± 1.73	12.44 ± 0.84
After NF	137 ± 16.2	<10*	68.72 ± 3.70
After RO	28 ± 6.7	<10*	93.61 ± 1.53
After RO-II	2**	<10*	99.54 ± 0.00
After EDI***	<0.1 (target)	—	>99.97

*TSS for NF and RO permeate was below the detection limit (< 10 mg/L).
Uncertainties are 1σ standard deviations propagated through removal calculations.
**2 μS/cm is the detection limit of the conductivity meter.
***EDI permeate quality reflects the manufacturer rating (Ionpure VNX50-3, Evoqua Water Technologies LLC, USA); not directly measured.

3.1 Hydraulic resistance

In general, the sum of R_m and R_f can be treated as a hydraulic resistance R_h, from a mechanical engineering viewpoint for pump selection.

Considering the driving force of the filtration steps TMP can be replaced by Δp. Based on the ion chromatographic analysis ion concentrations are extremely low at the RO stages, so $\Delta\pi$ can be neglected, from Eq. (5) then J_v can be simplified as follows:

$$J_v = \frac{\Delta p}{\mu \cdot R_h}, \tag{7}$$

where R_h is the hydraulic resistance. By rearranging Eq. (7), and using the definition for J_v in Eq. (3) and introducing Q as dV/dt the pressure drop can be calculated as follows:

$$\Delta p = \frac{\mu \cdot R_h}{A_m} \cdot Q, . \tag{8}$$

Viscosity rather depends on the temperature than salt concentration when considering the composition of Danube water and the permeate of each stage [24].

Treating the term permeate viscosity multiplied by the membrane resistance, divided by the membrane surface area, as a single factor yields a linear correlation between the applied pressure and the flow rate. Eq. (7) can be written as:

$$\Delta p = a \cdot Q, \tag{9}$$

where a is the hydraulic resistance factor [Pa·s/m^3].

To identify factor a, a set of Danube water filtration experiments was performed at different applied pressures for each membrane filtration step; the flow rate as a function of pressure. Pure water viscosity values were considered based at laboratory temperatures (21-23 °C) because after the permeate left the equipment, it was conditioned to the lab temperature. Different flow rates were observed for the different types of membranes at different applied pressures.

The linear correlation (shown in Fig. 6) observed between the flow rate and the applied pressure across all tested membranes confirms there is no significant fouling resistances. The flux is primarily governed by hydraulic resistance, as expected, which validates the linearity of Eq. (7).

The applied pressures were 4, 6, 8, and 10 bar for the UF membrane. Then, 14, 16, 18, and 20 bar for the NF membrane, and finally, 25, 28, 31, and 35 bar for the RO membrane. Based on Eq. (7), hydraulic resistance was calculated for each membrane step, showing a tendency while working under different pressures, see Fig. 7.

3.2 Lab-scale membrane filtration experiments

Pretreatment and desalination lab-scale experiments were conducted using several steps of membrane filtration techniques for pure water production, as displayed in Fig. 5. A circulation pump was used during each filtration step to maintain the cross-flow mode filtration. An EDI unit is theoretically added to achieve ultrapure water.

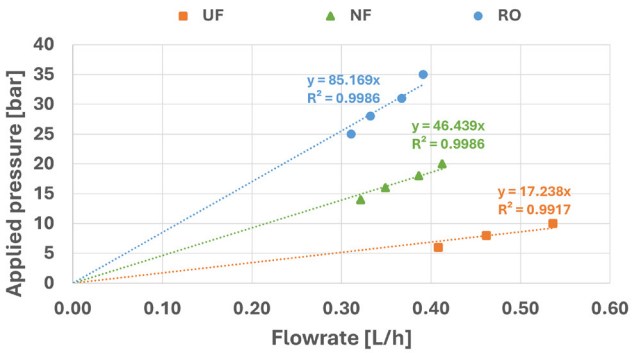

Fig. 6 Applied pressure drop versus flow rate for three types of membrane filtration (UF, NF, and RO) with an area of 28 cm^2 for Danube water at 25 °C

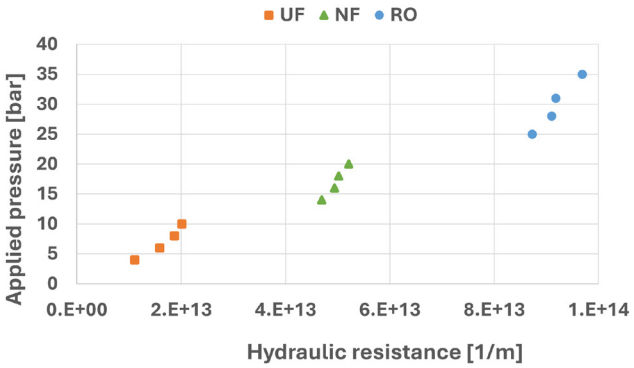

Fig. 7 Hydraulic resistance versus applied pressure for three types of membranes (UF, NF, and RO) with an area of 28 cm^2 for Danube water at 25 °C

Since the recovery of MF-I was 100%, 500 mL out of 500 mL of feed water was fed to MF-II stage. Further stages worked with 90%, 90%, 90%, 85% and 80% recoveries for MF-II, UF, NF, RO-I and RO-II, respectively when the permeate of a step was fed to the following step as feed. Therefore, 50% overall recovery (expressed as pure water) was obtained at the lab scale.

Fig. 8 presents the permeate flux of UF, NF, RO-I, and RO-II as a function of cumulative operating time for the batch filtration sequence, merging the four consecutive experiments into a single continuous plot. At the beginning of each filtration step, an initial high flux is observed, followed by a steady operation. When the initial transient period (the first 20% of recovery) is excluded, the remaining data show a linear decline throughout the treatment cascade treatment, as indicated by the fitted black line. This suggests that, under steady-state conditions, the flux decline across all membranes can be approximated by a single linear relationship with time, supporting the assumption that intrinsic membrane resistance governs the filtration process.

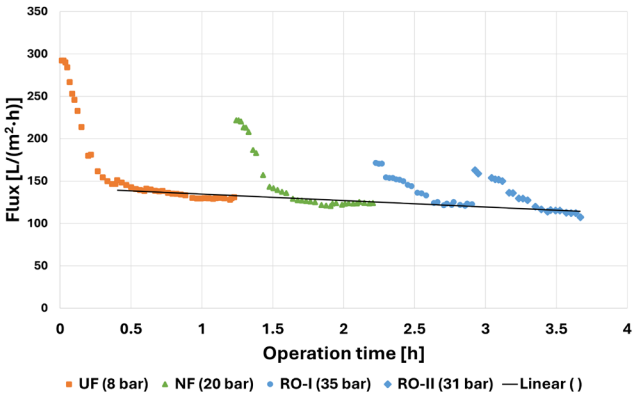

Fig. 8 Permeate flux as a function of cumulative operation time for the sequential batch filtration of Danube River water

Based on the lab-scale experiments, flow rate values were calculated for each step. These values were used to select the suitable pumps for the proposed industrial-scale filtration system.

The water produced as a permeate of RO-II has a conductivity of 2 µS/cm. Therefore, a further electrodeionization step is needed in the post-refining stage, to produce ultrapure water. When selecting an Ionpure VNX50-3 electrodeionization unit [25], the manufacturer specifies an operational recovery of 90–95% under a required inlet pressure of 1.4-7 bar.

3.3 Upscaling

Because of the pretreatment and desalination stages executed at a laboratory scale, upscaling calculations were needed and performed. Based on the make-up water requirements of one block of Paks power plant,, which needs 724.4 kg/s of superheated steam, we estimated the make-up water requirements [26] as 1% steam loss assumed in the energy conversion cycle. This amount should be compensated by make-up water. The estimation resulted in a make-up water requirement for this block as 26.1 m^3/h of ultrapure water. So, 26.1 m^3/h flow rate was used as a target flow rate as the permeate of the EDI unit, which was the first step of designing an industrial-scale ultrapure water production system.

3.3.1 Flow cascade and mass balance

Estimating the pure-water production requirements and the recovery of each step, the retentate and feed flow rate (marked with Q_R and Q_{Feed} in Table 3) of each step was calculated for the pump selection stage; in the case of EDI the permeate flow rate (marked with Q_P in Table 3) was assumed to be 26.1 m^3/h as mentioned before, and using 90% as a recovery, the feed flow rate of EDI – which represents the permeate of RO-II – was calculated accordingly (29 m^3/h). Using 90% recovery for the RO-I stage, a feed rate of 32.2 m^3/h was obtained, which also corresponds to the NF permeate flow rate. These calculations were continued, so feed flow rates of NF, UF, and MF-II were determined using 90% recovery for each step. Consequently, Table 3 summarizes the resulting flow cascade. The overall system recovery is 53.14%, yielding a raw Danube water feed of 49.11 m^3/h and a total reject stream of 23.01 m^3/h.

This low cumulative recovery is an inherent trade-off in multi-stage sequential membrane systems. While this ensures that the final permeate meets the strict target

Table 3 Flow cascade for the proposed industrial-scale ultrapure water system

Stage	Recovery (–)	Q_{Feed} (m³/h)	Q_P (m³/h)	Q_R (m³/h)	Cumulated reject (m³/h)	Pump ID
MF-I	1.00	49.11	49.11	0.00	0.00	—
MF-II	0.90	49.11	44.20	4.91	4.91	P1
UF	0.90	44.20	39.78	4.42	9.33	P1
NF	0.90	39.78	35.80	3.98	13.31	P2
RO-I	0.90	35.80	32.22	3.58	16.89	P3
RO-II	0.90	32.22	29.00	3.22	20.11	P4
EDI	0.90	29.00	26.10	2.90	23.01	P5

conductivity of 2 µS/cm prior to electrodialysis, it underscores the need for an abundant feedwater source, such as the Danube River, to make this configuration feasible. Other techniques can also be used to recycle the rejected feed into other filtration systems to reduce waste streams.

3.3.2 System process flow

The complete filtration sequence is presented; five pumps provide the hydraulic driving force, each assigned to a distinct pressure zone. The required membrane area for each stage ($A_{m,aim}$) was calculated from the laboratory-scale permeate flux at the selected operating pressure, as $A_{m,aim} = Q_P/J_v$. A safety factor SF = 1.3 was applied to account for concentration polarization development along the element channel. Under steady-state conditions the fouling resistance was negligible in the laboratory cell but it in spite of that it can be significant at industrial scale, therefore the hydraulic resistances combined with safety factor were used. Commercial spiral-wound membrane elements were then selected. The number of elements n and pressure vessels is determined from the element area and the manufacturer maximum elements-per-vessel (EPV) constraint. Table 4 summarizes the resulting configuration. Element models were selected as follows: GK4040F30 (SUEZ, France); NF270-4040 (DuPont, Water Solutions Company, USA); BW30 PRO-400/34i (DuPont, Water Solutions Company, USA); BW30 PRO-400/34i (DuPont, Water Solutions Company, USA) for UF, NF, RO-I and RO-II, respectively. During the iteration the maximum flow rate for each membrane was also another constraint, which resulted in a higher membrane area than the aimed one.

Regarding the post-treatment stage for EDI, three IonPure VNX50-3 modules in parallel, each rated at 5.7-17.0 m³/h were selected. The total feed of 29.00 m³/h is distributed as 9.67 m³/h per EDI module [27], which is within the operating range suggested by the manufacturer.

3.3.3 Pump selection

Five centrifugal pumps were selected, one per pressure zone, using the Grundfos Product Selector [28]. Shaft power was calculated using Eq. (10), where η is the pump efficiency [–] from the manufacturer's sizing software and P_{shaft} is the shaft power [W]. The International Electrotechnical Commission (IEC) motor frame standard was selected as the next standard size above $P_{shaft} \times 1.10$. Pumps P3 and P4 (Grundfos BMS HS series, Grundfos Hungary Ltd, Hungary) are complete high-pressure pump-and-motor packages designed for flooded inlet operation. Table 5 summarizes the selected pumps for each stage; for convenience, operating pressures are reported in bar and shaft powers in kW.

$$P_{shaft} = \Delta p \cdot Q / \eta \tag{10}$$

The total installed motor power for the whole process is 157 kW, and the total shaft power required is 132.57 kW. Pumps P3 and P4 are equipped with variable-frequency drives (VFDs) as required by the FilmTec BW30 PRO (Filmtech Company, now member of DuPont Water Solutions, USA) membrane start-up specification. Based on the water flow rate produced and the total motor power, the specific electric energy consumption for the whole system was determined to be 5.079 kWh/m³ pure water.

Table 4 Membrane element selection and area sizing (SF = 1.30 applied to $A_{m,aim}$), where $A_{m,elem}$ stands for the element area and $A_{m,real}$ stands for the real membrane area, calculated as a product of n total and $A_{m,elem}$

Stage	Δp [bar]	$A_{m,aim}$ (m²)	Vessels	EPV	n total	$A_{m,elem}$ (m²)	$A_{m,real}$ (m²)
UF	8	268	15	3	45	7.9	355.5
NF	20	270	12	4	48	7.6	364.8
RO-I	35	256	5	2	10	37.0	370
RO-II	31	246	3	3	9	37.0	330

Table 5 Selected pumps for the industrial-scale ultrapure water system (P_{shaft} stands for the shaft power and Motor represents the electric power need of each pump. Model types are selected from Grundfos pump supplier, Gundfos Hungary Ltd., Hungary)

ID	Duty	Q (m³/h)	Δp [bar]	η (–)	P_{shaft} (kW)	Motor (kW)	Model
P1	MF-II + UF feed	49.11	9	0.757	16.22	18.5	CRN 45-5
P2	NF feed	39.78	20	0.772	28.63	37	CRN 45-10-2
P3	RO-I feed	35.80	35	0.757	47.04	52	BMS 18-14 HS
P4	RO-II feed	32.22	31	0.773	36.51	44	BMS 18-11 HS
P5	EDI booster	29.00	3	0.580	4.17	5.5	CRN 20-4

4 Conclusion

This study proposed, designed, and evaluated a multistage membrane filtration system to produce 26.1 m³/h of ultrapure water from Danube River water, suitable as make-up water for thermal power plants. Laboratory-scale experiments were conducted on various membranes (UF, NF, and RO) to assess the total resistances of the membranes at different operating pressures which were identified as hydraulic resistances. The experimental results confirmed a linear correlation between permeate flow rate and applied pressure for all three types of membranes and in the steady state cascade operation validating that the hydraulic resistance governs the filtration process, with negligible fouling and concentration polarization resistances.

Industrial-scale sizing was based on experimental results, and the flow cascade was modeled to meet the 26.1 m³/h ultrapure water requirements for one block of Paks power plant. The proposed configuration consists of pretreatment, a desalination sequence, and EDI as post-treatment to achieve ultrapure water.

The overall cumulative recovery of the system is 53.14%, requiring a raw water intake of 49.11 m³/h to achieve the target ultrapure water production. While this recovery is necessary to achieve the 0.08 µS/cm conductivity target, it underscores the need for an abundant water source, such as the Danube River. Five centrifugal pumps were chosen to provide the necessary hydraulic driving force across the configuration, with a total shaft power required to drive the system of 132.57 kW and a system specific electric energy consumption of 5.079 kWh/m³ of ultrapure water produced.

This work provides the basis for scaling a laboratory membrane cascade system to an industrial scale and can serve as an aid for preliminary system sizing. The topic covers interdisciplinary work between chemical and mechanical engineering aspects. Future work could explore recycling the rejected feed streams to improve recovery and reduce water withdrawal.

Acknowledgement

The project was supported by the Hungarian National Research, Development and Innovation Office (NKFIH) under Project Number FK-143215. The authors thank the Department of Chemical and Environmental Process Engineering at Budapest University of Technology and Economics for providing lab facilities for these experiments. The authors thank Hasan Algburi and Faranak Soltani, MSc students in the lab experiments. The authors appreciate the help of Prof. Csaba Hős in the pump selection.

The research was funded by the Sustainable Development and Technologies National Program of the Hungarian Academy of Sciences (FFT NP FTA).

References

[1] Pororov, S. A., Kornilova, N., Platonov, K. "Ultra pure water: Intensive water demineralisation through ion exchange", Filtration + Separation, 48(2), pp. 36–39, 2011. https://doi.org/10.1016/S0015-1882(11)70085-4

[2] Shaheen, R. "Make-up water preparation of power plants", PhD Thesis, Budapest University of Technology and Economics, 2024. Available at: http://hdl.handle.net/10890/57832 [Accessed: 01 March 2026]

[3] Hube, S. "Direct Membrane Filtration of Municipal Wastewater: Linking Periodical Physical Cleaning with Fouling Mechanisms", MSc Thesis, University of Iceland, 2020.

[4] Espinasse, B., Bacchin, P., Aimar, P. "On an experimental method to measure critical flux in ultrafiltration", Desalination, 146(1–3), pp. 91–96, 2002. https://doi.org/10.1016/S0011-9164(02)00495-2

[5] Kusworo, T. D., Yulfarida, M., Kumoro, A. C., Utomo, D. P., Aryanti, N. "Effect of Nanophotocatalyst WO3 Addition on PVDF Membrane Characteristics and Performance", Periodica Polytechnica Chemical Engineering, 68(3), pp. 338–347, 2024. https://doi.org/10.3311/PPCH.24008

[6] Doran, P. M. "Unit Operations", In: Bioprocess Engineering Principles, Elsevier, 2013, pp. 445–595. ISBN 978-0-12-220851-5 https://doi.org/10.1016/B978-0-12-220851-5.00011-3

[7] Kim, A. S., Kim, H., Kim, A. S., Kim, H. "Membrane Thermodynamics for Osmotic Phenomena", In: Yonar, T. (ed.) Desalination, InTech, 2017. ISBN 978-953-51-4689-6 https://doi.org/10.5772/intechopen.68406

[8] Abdelrasoul, A., Doan, H., Lohi, A. "Fouling in Membrane Filtration and Remediation Methods", In: Nakajima, H. (ed.) Mass Transfer - Advances in Sustainable Energy and Environment Oriented Numerical Modeling, InTech, 2013. ISBN 978-953-51-6356-5 https://doi.org/10.5772/52370

[9] Ripperger, S., Gösele, W., Alt, C. "Filtration, 1. Fundamentals", In: Ullmann's Encyclopedia of Industrial Chemistry, Wiley, 2009. ISBN 9783527306732 https://doi.org/10.1002/14356007.b02_10.pub2

[10] Syahidah Zafisah, N., Lun Ang, W., Wahab Mohammad, A. "Cake Filtration For Suspended Solids Removal in Digestate From Anaerobic", Water Conservation and Management (WCM), 2(1), pp. 5–9, 2018. https://doi.org/10.26480/wcm.01.2018.05.09

[11] Aguirre-Montesdeoca, V., Janssen, A. E. M., Van der Padt, A., Boom, R. M. "Modelling ultrafiltration performance by integrating local (critical) fluxes along the membrane length", Journal of Membrane Science, 578, pp. 111–125, 2019. https://doi.org/10.1016/j.memsci.2019.02.040

[12] Wijmans, J. G., Baker, R. W. "The solution-diffusion model: a review", Journal of Membrane Science, 107, (1–2), pp. 1–21, 1995. https://doi.org/10.1016/0376-7388(95)00102-I

[13] Iritani, E. "A Review on Modeling of Pore-Blocking Behaviors of Membranes During Pressurized Membrane Filtration", Drying Technology, 31(2), pp. 146–162, 2013. https://doi.org/10.1080/07373937.2012.683123

[14] Di Bella, G., Di Trapani, D. "A Brief Review on the Resistance-in-Series Model in Membrane Bioreactors (MBRs)", Membranes, 9(2), 24, 2019. https://doi.org/10.3390/membranes9020024

[15] Tracey, E. M., Davis, R. H. "Protein Fouling of Track-Etched Polycarbonate Microfiltration Membranes", Journal of Colloid Interface Science, 167(1), pp. 104–116, 1994. https://doi.org/10.1006/jcis.1994.1338

[16] Zakar, M., Farkas, D. I., Hanczné-Lakatos, E., Keszthelyi-Szabó, G., László, Z. "Purification of Model Dairy Wastewaters by Ozone, Fenton Pre-treatment and Membrane Filtration", Periodica Polytechnica Chemical Engineering, 64,(3), pp. 357–363, 2020. https://doi.org/10.3311/PPCH.15046

[17] Tansel, B., Sager, J., Garland, J., Xu, S. "Effect of transmembrane pressure on overall membrane resistance during cross-flow filtration of solutions with high-ionic content", Journal of Membrane Science, 328(1–2), pp. 205–210, 2009. https://doi.org/10.1016/j.memsci.2008.12.003

[18] Maczyszyn, A. "Investigation Method And Mathematical Model of Pressure Losses in Hydraulic Rotary Motor", Polish Maritime Research, 25(1), pp. 93–98, 2018. https://doi.org/10.2478/pomr-2018-0011

[19] Shaheen, R., Cséfalvay, E. "The Role of Coagulation and Microfiltration in Seawater Pre-treatment", Periodica Polytechnica Chemical Engineering, 66(4), pp. 557–564, 2022. https://doi.org/10.3311/PPCH.20025

[20] Torma, C. Z., Cséfalvay, E. "Nanofiltration: a Final Step in Industrial Process Water Treatment", Periodica Polytechnica Chemical Engineering, 62(1), pp. 68–75, 2018. https://doi.org/10.3311/PPCH.10640

[21] Huber, M. L., Perkins, R. A., Laesecke, A., Friend, D. G., Sengers, J. V., Assael, M. J., Metaxa, I. N., Vogel, E., Mareš, R., Miyagawa, K. "New International Formulation for the Viscosity of H_2O", Journal of Physical and Chemical Reference Data, 38(2), pp. 101–125, 2009. https://doi.org/10.1063/1.3088050

[22] Shaheen, R., Cséfalvay, E. "The effect of pretreatment and the operating temperature on reverse osmosis in make-up water preparation", Water Resources and Industry, 31, 200244, 2024. https://doi.org/10.1016/j.wri.2024.100244

[23] Kusworo, T. D., Veda, A., Mafazan, R., Hasbullah, H., Puspa, M. B. "Integrated Ozonation–Adsorption Pretreatment and Polyvinylidene Fluoride/Tungsten Based Polyoxometalate Photocatalytic Membrane for Produced Water Treatment", Periodica Polytechnica Chemical Engineering, 70(1), pp. 30–41, 2026. https://doi.org/10.3311/PPCH.42654

[24] Csefalvay, E. "Membrane Operations in the Green Technology: Solvent Recovery and Process Water Treatment Edit Cséfalvay", PhD Thesis, Budapest University of Technology and Economics, 2009.

[25] Evoqua Water Technologies "IONPURE VNX MODULE - VNX50-3", 2014. [online] Available at: www.lenntech.com [Accessed: 03 March 2026]

[26] Büki, G. "A Paksi Atomerőmű telítettgőz-körfolyamata" (The Saturated Steam Cycle at the Paks Nuclear Power Plant), In: Erőművek, Budapest: Műegyetemi Kiadó, 2004, pp. 164–165. (in Hungarian)

[27] Hajagos, S., Kovács, J. G. "Polymer-based Bipolar Plates for Fuel Cells: Design, Simulation, and Manufacturing", Periodica Polytechnica Mechanical Engineering, 69(1), pp. 40–45, 2025. https://doi.org/10.3311/PPME.38589

[28] Grundfos "Advanced Selection | Grundfos", [online] Available at: https://product-selection.grundfos.com/advanced-selection?sQcid=2901348544 [Accessed: 29 March 2026]